

Suppression of microwave magnetic envelope solitons by continuous wave magnetostatic wave signals

Mark M. Scott,^{a)} Yuri K. Fetisov, Valeri T. Synogach, and Carl E. Patton
Department of Physics, Colorado State University, Fort Collins, Colorado 80523

(Received 9 June 2000; accepted for publication 12 July 2000)

The influence of continuous wave (cw) magnetostatic wave signals on microwave magnetic envelope soliton pulse formation and propagation in magnetic films has been examined. Pulsed and cw microwave signals were applied to the input of a single crystal yttrium-iron-garnet film magnetostatic wave delay line. The nominal operating frequency was 4.8 GHz. The pulse signals served to form solitons with no cw power present. Under suitable conditions, the cw signal served to inhibit or eliminate the soliton formation and propagation. The suppression effect was measured as a function of the cw signal frequency and power. The suppression is maximized when the cw signal frequency coincides with the pulse carrier frequency. At this frequency, an input cw power of 80 mW is sufficient to suppress completely a soliton pulse formed from a 10 ns wide, 500 mW peak power input pulse. © 2000 American Institute of Physics. [S0021-8979(00)04320-6]

I. INTRODUCTION

The observation of microwave magnetic envelope (MME) solitons in thin yttrium-iron-garnet (YIG) films was first reported by Kalinikos, *et al.*¹ Since this discovery, there have been numerous studies of basic MME soliton properties.² There has been some limited work on soliton collisions^{3,4} and soliton formation due to the interaction of cw magnetostatic wave signals.⁵⁻⁷ However, there has been no work reported on the interactions between MME solitons and cw magnetostatic wave signals.

This article presents experimental results on the effect of cw magnetostatic wave (MSW) signals on MME solitons. One finds that a relatively low power cw MSW signal can effectively suppress MME soliton formation and propagation if the cw frequency is close to the soliton carrier frequency. Section II summarizes the measurement system and the experimental procedure. Section III presents the results. Section IV gives a brief summary of the results, a comment on possible device applications, and remarks on theoretical connections.

II. EXPERIMENT

Figure 1 shows a schematic diagram of the microwave measurement system. There are two microwave sources A and B, a fast microwave switch, a power amplifier, a phase shifter, two directional couplers DC1 and DC2, a YIG film magnetostatic wave delay line, and a signal analyzer. The delay line consisted of an 8.7- μm -thick YIG film and a pair of 50- μm -wide microstrip transducer elements separated by 3.8 mm. The YIG film is indicated by the gray rectangular strip. The transducers are indicated by the thin black lines beneath the strip. A magnetic field of 1038 Oe was applied along the length of the YIG strip and the MSW propagation direction, as indicated. Microwave source A, the switch, and

the amplifier were used to produce narrow high power microwave pulses. These pulses were applied to the input of the delay line in order to form solitons. Source B, in conjunction with the phase shifter, was used to produce a phase variable cw signal. Source A was operated at 4.8 GHz for the results given below.

The delay line arrangement given above, with propagation parallel to the magnetic field, corresponds to the magnetostatic backward volume wave (MSBVW) configuration. The use of the MSBVW configuration for MME soliton formation and propagation in YIG film delay lines is discussed in Refs. 3 and 8. In brief, for the MSBVW arrangement, the nonlinear frequency response and the dispersion combine to support soliton formation for narrow microwave pulses at appropriate power levels applied to the input of the delay line. For an applied field of 1038 Oe and a frequency of 4.8 GHz indicated above, one obtains MSBVW pulse or cw signals propagating at a wave number k of approximately 200 rad/cm. The corresponding wavelength, $2\pi/k \approx 300 \mu\text{m}$, provides a reasonable match to the transducer element width given above.

The microwave amplifier had a bandwidth greater than 5 GHz, a 30 dB dynamic range, and a high peak power. This ensured that the observed output pulse characteristics were determined by the YIG film and MSBVW response characteristics only. The pulse repetition rate was set at 1 kHz. For the source B signal, both cw and 10 ms long pulses at the MSW pulse signal repetition rate were used and the same overall results were obtained. This eliminated the possibility of heating effects.

The arrangement described above was used first to excite MSBVW solitons and then to observe the effect of the cw signal on the soliton output pulse. For the soliton generation, the pulse width was set at 10 ns. As the pulse power was increased, the output pulse showed the characteristic steepening and narrowing associated with MME solitons.^{1-4,8} Output pulse phase profiles⁹ and peak output power versus

^{a)}Electronic mail: mscott@lamar.colostate.edu

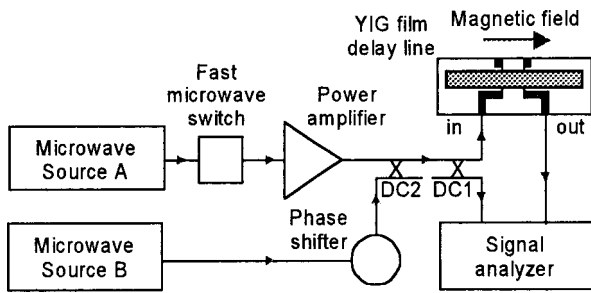


FIG. 1. Schematic diagram of the microwave measurement system.

input power response curves¹⁰ were used to verify soliton formation and propagation.

Once the soliton pulse response was obtained, source B was used to introduce a cw MSBVW signal into the YIG film delay line. The soliton output power versus time profile was then monitored as a function of the cw power level and the cw signal frequency. The influence of the relative phase of the cw signal was also observed for the above measurements. Source B could provide power levels up to about 200 mW at the input transducer.

The results of these measurements are given below. For clarity, a specific nomenclature for the various power levels in the experiment is adopted. The peak power for the input pulse at the delay line input will be denoted as P_{pulse}^{in} . The corresponding pulse peak power at the delay line output will be denoted as P_{pulse}^{out} . The cw power level at the delay line input will be denoted as P_{cw}^{in} . The corresponding cw power level at the delay line output will be denoted as P_{cw}^{out} .

III. RESULTS

Figure 2 shows typical results of the MSBVW pulse measurements for low and high input pulse power levels, with and without cw power applied to the delay line. All graphs show output power versus time. The left side graphs under (a) are for no cw power applied. The right side graphs under (b) are for nonzero levels of cw power, as indicated. The top row graphs are for a low power input pulse at $P_{pulse}^{in} = 3\text{ mW}$. This power level is well below the soliton threshold. The bottom row graphs are for $P_{pulse}^{in} = 500\text{ mW}$. This power level is above the soliton threshold. The pulse carrier frequency and the cw frequency were both set at 4.8 GHz for these measurements. As indicated above, the cw phase was set to optimize the effect of the cw signal on the pulse response for the panel (b) graphs. Note that the values of P_{cw}^{in} are different for the top and bottom graphs in panel (b). The effect of P_{cw}^{in} on the pulse and cw output response will be considered at the end of this section.

The data in Fig. 2 show the essential features of the soliton suppression effect. The top graphs in (a) and (b) show that the cw signal has an effect, even for a low power dispersive MSW pulse. The dispersed pulse in (a) for no cw power changes to show an oscillatory character, as in (b), when there is low power cw signal applied. This, however, is clearly a linear effect. The different phase shifts experienced by the Fourier components of the dispersive pulse interact with the fixed phase cw signal to produce the signal envelope

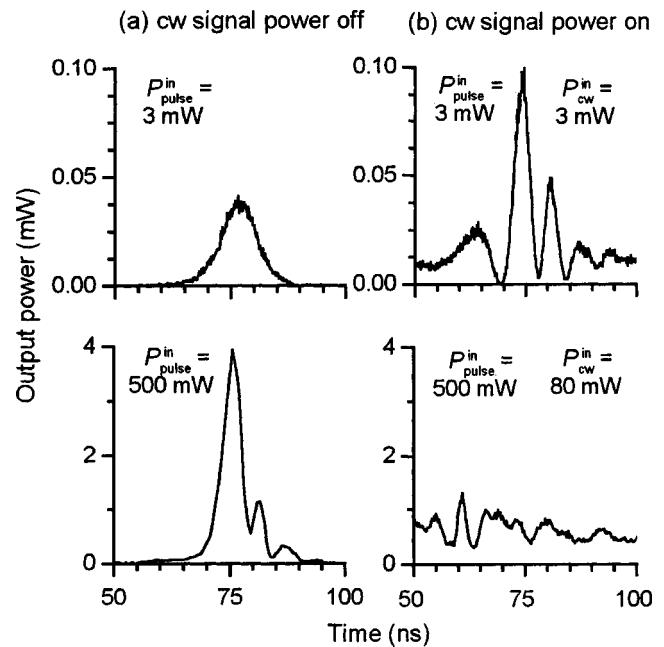


FIG. 2. Profiles of delay line output power vs time for 10-ns-wide input pulses. Panels (a) and (b) are for no applied cw power and nonzero power levels as indicated by the P_{cw}^{in} values for the right side graphs, respectively. The top and bottom row graphs are for different values of the input peak power level P_{pulse}^{in} , as indicated.

shown in the top graph in (b). The bottom graphs in (a) and (b), obtained for soliton pulse propagation, show a nonlinear effect. Here, one sees that the cw signal has essentially destroyed the soliton pulse. There is still a small oscillatory output signal, but this is much weaker than the original soliton pulse.

For the dispersive pulse in (a) the interaction with any nonzero cw power level P_{cw}^{in} in the linear regime produced an oscillatory result similar to that shown in (b). For the soliton, however, the suppression is not observable until the cw input signal power level P_{cw}^{in} reaches about 1 mW. As the cw signal power is increased, the soliton pulse peak output power P_{pulse}^{out} decreases in a nonlinear fashion. During this decrease, the soliton pulse envelope shows an oscillatory character which depends on the relative phase of the two signals. Even when the soliton pulse peak output power P_{pulse}^{out} becomes very small, this phase dependent oscillation remains. It is important to note, however, that the general suppression effect was observed for all values of the cw signal phase relative to the pulse signal.

Figure 3 shows further details on the output pulse peak power and output cw power levels as a function of the input cw power level. The upper set of data points show that there is a critical value of the input cw power P_{cw}^{in} of about 0.5–1 mW which is needed to reduce the soliton peak response. As the cw power P_{cw}^{in} is increased, the pulse peak output power P_{pulse}^{out} decreases in a highly nonlinear manner. The decrease in P_{pulse}^{out} is strongest for P_{cw}^{in} in the range 1–10 mW where P_{cw}^{in} is still linear. For P_{cw}^{in} values in the 50 mW range, the soliton suppression is virtually complete. Keep in mind that all data shown here are for an input pulse peak power level of 500 mW.

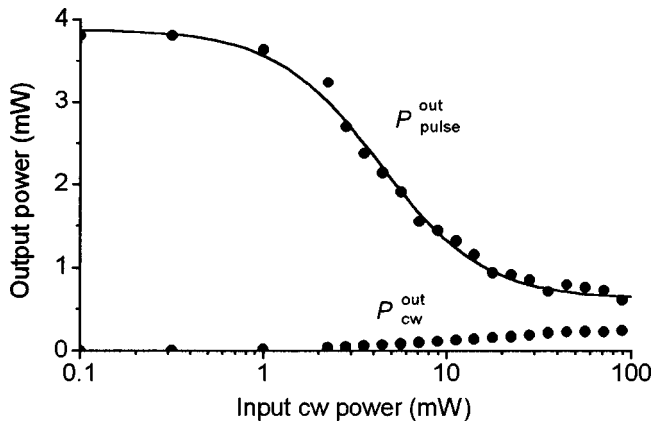


FIG. 3. Output pulse peak power $P_{\text{pulse}}^{\text{out}}$ and cw output power $P_{\text{cw}}^{\text{out}}$ as a function of input cw power $P_{\text{cw}}^{\text{in}}$.

Finally, turn to the effect of the cw frequency on the suppression effect. Figure 4 shows typical frequency data. Graph (a) gives the Fourier power spectrum for the soliton output pulse signal for no cw power on the line. Graph (b) gives the variation in the soliton pulse peak output power as a function of the cw signal frequency, with the cw input power held constant at 80 mW. As with previous data, the peak power for the input pulse, $P_{\text{pulse}}^{\text{in}}$, was held at 500 mW. The vertical axis in (a) is shown in logarithmic scale. The solid curve in graph (b) is only a guide to the eye. The scatter in the data arises due to the oscillatory behavior of the suppression effect. Similar measurements were made for lower cw powers. The effect was the same, except that the level of the maximum suppression was less for lower cw powers, as in Fig. 3.

The results in Fig. 4 establish two additional features of the soliton suppression effect. First, the suppression is most effective when the cw signal frequency coincides with the input pulse carrier frequency of 4.8 GHz. Second, one sees

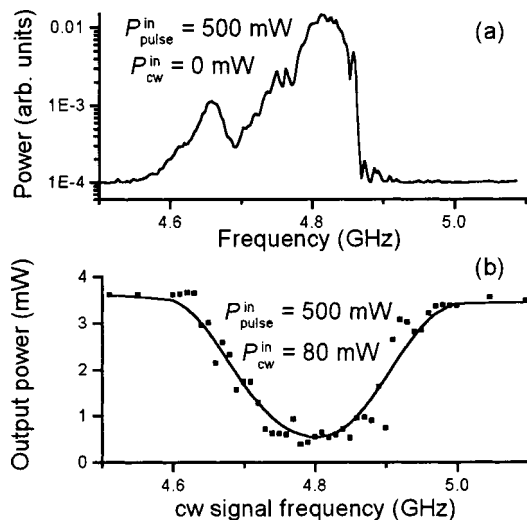


FIG. 4. Graph (a) shows the Fourier power spectrum for the soliton output pulse with no cw signal applied to the line. Graph (b) shows the output pulse peak power $P_{\text{pulse}}^{\text{out}}$ for the soliton pulse as a function of the cw signal frequency with the cw signal power $P_{\text{cw}}^{\text{in}}$ held constant at 80 mW. The solid line in (b) is only a guide to the eye.

that the bandwidth for the suppression matches the 200 MHz width of the power spectrum for the original soliton pulse. As an additional point of interest, one may note that the soliton pulse carrier frequency and the frequency for maximum suppression do not coincide with the peak in the soliton pulse power spectrum. This peak in the spectrum is shifted somewhat above the 4.8 GHz frequency point. From the soliton profile in the lower left graph of Fig. 2, one can see two additional small peaks after the main peak. These peaks are an indication of a small higher order soliton response.¹⁰ The effect of these peaks is to shift the peak in the power spectrum to higher frequency and to alter the spectrum from the hyperbolic secant shape characteristic of single solitons. However, the observed soliton suppression is a general soliton effect which is not limited to higher order solitons but is observed for both single and higher order solitons.

Qualitatively similar results were achieved with the same 8.7- μm -thick film oriented in the magnetostatic forward volume wave configuration and for a 10.2- μm -thick film in the MSBVW configuration.

IV. SUMMARY AND CONCLUSIONS

The results given above demonstrate that a relatively low power cw MSW excitation can inhibit or eliminate MME soliton pulse propagation in magnetic films. The suppression effect occurs for a band of cw frequencies which match the power spectrum of the soliton pulse. The suppression effect is optimized when the soliton carrier frequency and the cw signal frequency coincide.

The control of soliton pulse properties through cw power may be useful for microwave signal processing device applications. One possible configuration for such a device consists of a ‘‘soliton valve’’ in which a small cw microwave power is used to turn on or off the propagating soliton pulse or sequence of pulses from a soliton train generator.⁷

The results given here are experimental only. A quantitative theory to explain these results is needed. It should be possible to perform numerical calculations based on two coupled nonlinear Schrödinger (NLS) equations for the pulse response to a cw MSW signal. It has been possible to model MME solitons through the NLS equation.¹¹ It should also be possible to use coupled NLS equations, for example, to model the new effects reported above.

ACKNOWLEDGMENTS

This work was supported in part by the National Science Foundation, Grant No. DMR-9801649, and the U. S. Army Research Office, Grant No. DAAG55-98-1-0430. The film was provided by Dr. J. D. Adam, Electronic Sensors and Systems Division, Northrop Grumman Corporation, Baltimore, Maryland. Part of the work by CEP was done at the University of Kaiserslautern, Germany, under partial support from the Alexander von Humboldt Foundation.

¹B. A. Kalinikos, N. G. Kovshikov, and A. N. Slavin, *Pis'ma Zh. Eksp. Teor. Fiz.* **94**, 159 (1988) [*JETP Lett.* **67**, 303 (1988)].

²C. E. Patton, P. Kabos, H. Xia, P. A. Kolodin, H. Y. Zhang, R. Staudinger, B. A. Kalinikos, and N. G. Kovshikov, *J. Magn. Soc. Jpn.* **23**, 605 (1999).

- ³N. G. Kovshikov, B. A. Kalinikos, C. E. Patton, E. S. Wright, and J. M. Nash, *Phys. Rev. B* **54**, 15210 (1996).
- ⁴O. Büttner, M. Bauer, S. O. Demokritov, B. Hillebrands, M. P. Kostylev, B. A. Kalinikos, and A. N. Slavin, *Phys. Rev. Lett.* **82**, 4320 (1999).
- ⁵V. E. Demidov, *Pis'ma Zh. Eksp. Teor. Fiz.* **68**, 828 (1998) [*JETP Lett.* **68**, 869 (1998)].
- ⁶B. A. Kalinikos, M. M. Scott, and C. E. Patton, *Phys. Rev. Lett.* **84**, 4697 (2000).
- ⁷B. A. Kalinikos, N. G. Kovshikov, and C. E. Patton, *Phys. Rev. Lett.* **80**, 4301 (1998).
- ⁸M. Chen, M. A. Tsankov, J. M. Nash, and C. E. Patton, *Phys. Rev. B* **49**, 12773 (1994).
- ⁹J. M. Nash, P. Kabos, R. Staudinger, and C. E. Patton, *J. Appl. Phys.* **83**, 2689 (1998).
- ¹⁰J. M. Nash, C. E. Patton, and P. Kabos, *Phys. Rev. B* **51**, 15079 (1995).
- ¹¹H. Y. Zhang, P. Kabos, H. Xia, R. Staudinger, P. A. Kolodin, and C. E. Patton, *J. Appl. Phys.* **84**, 3776 (1998).